Int. J. Multiphase Flow Vol. 13, No. 3, pp. 283–294, 1987
Printed in Great Britain.

0301-9322/87 $3.00 + 0.00

TRANSITION CRITERIA FOR TWO-PHASE FLOW PATTERNS IN VERTICAL UPWARD FLOW

Z. BILICKI† and J. KESTIN
Division of Engineering, Brown University, Providence, RI 02912, U.S.A.

(*Received* 15 *February* 1986; *in revised form* 15 *October* 1986)

Abstract—The present paper advances three simple models and uses them to determine, semi-heuristically, the transition criteria from bubble to slug flow and from slug to froth flow. The bubble–slug transition is assumed to be governed by a criterion which expresses the conditions under which two aligned bubbles are driven to coalesce by the velocity field in the wake of the forward bubble, which is translated into a criterion on separation between bubbles. The slug–froth transition is thought to occur by one of two mechanisms. The first one is also a criterion of coalescence, resulting in the determination of a critical separation l_*. The second is supposed to occur when the thin film between the wall and a Taylor bubble becomes unstable. Of the two mechanisms, the second prevails when the distance between two Taylor bubbles exceeds the critical value l_*. The results, interpreted broadly, agree well with those of Taitel *et al.*, but the impression that the field is in need of much further development cannot be ignored. The equations make it possible to study the sensitivity of the boundaries to pipe diameter, bubble diameter and fluid properties. A sample map in the usual U_{LS} vs U_{GS} coordinates is presented.

1. INTRODUCTION

An ability to predict the flow pattern which will be observed under given circumstances in two-phase flow constitutes one of the basic unsolved problems in this subject. The literature contains a number of so-called "maps", notably those propounded by Griffith & Wallis (1961) and Taitel *et al.* (1980), but the view prevails that they leave much to be desired. All, except Griffith and Wallis, employ dimensional coordinates consisting of the superficial velocities U_{LS} vs U_{GS}, whereas more general, dimensionless variables would be preferred. A study of the literature convinces one that the subject is intrinsically quite complex and that a proven, adequate set of parameters which determine the pattern remains to be discovered.

An experimental investigation carried out by Bilicki (1987) has clearly pointed to the fact that the field overlaps the field of slug flow, the pattern in the transition region depending on the manner of air injection. This and other investigations confirm that pattern boundaries in U_{LS}, U_{GS} coordinates cannot possibly be sharp that the discrepancies between different investigations may often be attributed to unidentified influences rather than faults in the respective techniques of experimentation.

In the face of such a complex and largely unresolved state of affairs, it is still useful to attempt to interpret experimental data analytically. The present paper makes just such an attempt and chooses two very simple, not to say crude, models for the bubble–slug and slug–froth transitions. The structure of these simple models is inspired to a large extent by direct observation (Bilicki 1987) and the conventional representation in terms of superficial velocities is retained *faute de mieux*. The analysis leads to a satisfactory (by the present standards of this topic) agreement with observations.

Although the experimental content underlying this study is based on work with air-injected water, it is expected, not asserted, that the same boundaries exist in the presence of a phase transition. However, the results are definitely not applicable other than to the vertical upward-flow case described in Bilicki's investigation.

2. TRANSITION FROM BUBBLE TO SLUG FLOW

In order to estimate the point of transition between bubble and slug flow, we adopt the following

†Permanent address: Institute for Fluid Flow Machinery, Polish Academy of Science, Gdansk, Poland.

physical model. Bubble flow consists of an array of spherical gaseous elements which are dispersed over a liquid stream. The bubbles move upwards through the vertical channel with a velocity which exceeds that of the adjacent liquid. This relative slip causes a perturbation of the basic flow pattern and gives rise to a wake behind each bubble. The mean fluid velocity in each wake is also higher than that in the adjacent liquid. In some parts of the flow field there occur situations in which a bubble (say bubble No. 1 in figure 1) follows another bubble (bubble No. 2) and accelerates in the wake of No. 1. This creates a tendency for bubbles to catch up with predecessors and to coalesce. If the distance, a, between two bubbles of which one trails the other exceeds a certain characteristic (or effective) length l, the two cease to interact, and the tendency to coalesce is absent. For values of $a < l$ this tendency exists, bubbles coalesce, and eventually form Taylor bubbles. From the practical point of view, the transition is not sharp, because both quantities, i.e. a and l, are stochastic in nature and follow a probability distribution which is approximately Gaussian (Bilicki 1987; Sekoguchi *et al.* 1981).

In the model under consideration, it has been assumed that transition occurs when the statistical (or ensemble) averages $\bar{l}$ and $\bar{a}$ of the above two quantities become equal. It is clear that the absolute velocity of a bubble has an axial as well as a radial component. In our model the assumption is made that the radial displacement of a bubble does not lead to coalescence and that only the axial component counts, as was observed visually in Bilicki's loop.

We begin our analysis by considering a single spherical body which is dragged through a stationary fluid with a velocity U_∞, thus creating a wake behind it, figure 2. We assume that the velocity distribution $u(z, r)$ in the wake is adequately described by Prandtl's theory of turbulent wakes and von Karman's similarity hypothesis (Schlichting 1979, pp. 585, 734). Essentially, this theory amounts to a dimensional analysis which is based on several well-proven physical

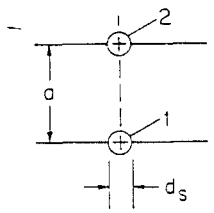

Figure 1. Notation.

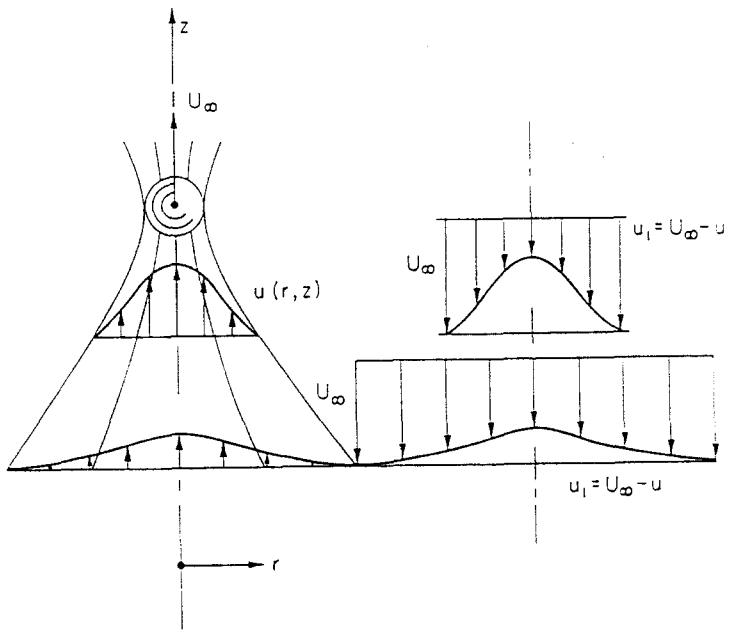

Figure 2. Sphere dragged with velocity U_∞ through fluid at rest. (Wake relative to liquid when sphere moves with a relative velocity.)

hypotheses and leads to the conclusions that the velocity $u_l(z, r)$ in the wake measured relative to the moving sphere,

$$u_l = U_\infty - u, \tag{1}$$

is proportional to the group

$$u_l \sim U_\infty \left(\frac{C_D d_S^2}{\beta^2 z^2}\right)^{1/3}. \tag{2}$$

Here C_D, is the drag of the sphere and β is a constant of proportionality between the mixing length of the flow and the diametral width of the jet (Schlichting 1979, p. 742). The coefficient of proportionality between u_l and the dimensionless group depends on r, and assumes some, as yet unspecified value when u_l is measured along the flow axis, z.

It is clear that in this model U_∞ represents the slip velocity,

$$U_\infty = \frac{U_{GS}}{\alpha} - \frac{U_{LS}}{1-\alpha}. \tag{3}$$

Furthermore, it is hypothesized that the wake terminates when u_l becomes equal to the local friction velocity v_*, as measured by Theofanous & Sullivan (1982). The friction velocity is a measure of the velocity fluctuations in the liquid, and when the wake velocity attains the same magnitude,

$$u_l = v_*, \tag{4}$$

the pull of the wake ceases. Thus, transcribed in our notation, we put

$$\left[\frac{v_*(1-\alpha)}{U_{LS}}\right]^2 = \frac{\left[\frac{1}{2} f(1-\alpha^2) + 4\alpha(1-\alpha)\left(1-\frac{\rho_G}{\rho_L}\right)\frac{Dg(1-\alpha)^2}{4\,U_{LS}^2}\right]}{\left(1+1.5\alpha\frac{D}{d_S}\right)}. \tag{5}$$

Here D is the channel diameter, f is the friction factor for the liquid, and the coefficient δ which appears in [19] of Theofanous & Sullivan has been assigned the value $\delta = 4$, i.e. close to the upper limit of $\delta \sim 2$ to 4.5 recommended. Similarly a constant value $f = 0.01$ has been assumed, corresponding to a relative roughness of 10^{-2} (Schlichting 1979, p. 624, $f = \frac{1}{4}\lambda$). Both numerical assumptions will be justified *ex post*.

If a bubble is aligned with the wake of a preceding bubble, it will be drawn in if $v_* < u_l$, and the attraction will cease for $v_* = u_l$ sufficiently closely. The length l which corresponds to this situation, figure 3, will satisfy [2] and [4].

Combining [2] with [4], and replacing the distance z with the limiting distance l, we derive that

$$\frac{l}{d_S} = A_1 \frac{C_D^{1/2}\, U_\infty^{3/2}}{v_*^{3/2}}. \tag{6}$$

Here A_1 is a coefficient, to be determined experimentally. We assume that this ratio adequately approximates the ratio of stochastic averages $\bar{l}/\bar{d}_S$.

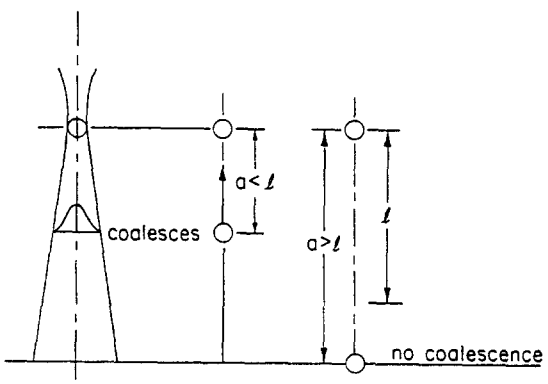

Figure 3. Conditions for presence and absence of coalescence of two spheres.

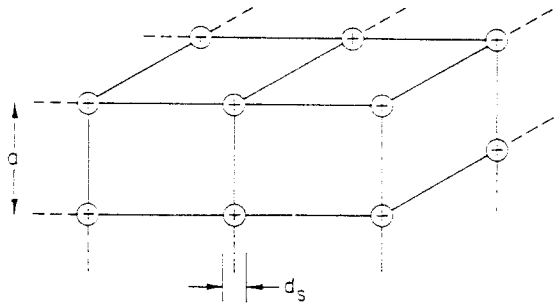

Figure 4. Array for the calculation of the stochastic distance ratio $\bar{a}/\bar{d}_S$.

It is clear that the void fraction, α, must be related to the stochastic value, $\bar{d}_S$, of the bubble diameter for a given pipe diameter, and the distance $\bar{a}$ and spatial distribution of bubbles interpreted in a stochastic sense. Supposing the system is ergodic, we assume a regular array and postulate that the result remains valid for actual configurations. The recommended array is shown in figure 4. In it the bubbles simply place themselves at the vertices of cubes. The ratio a/d_S for this and other (discarded) arrays was compared with extensive photographs from which the frequency of pairs of bubbles was plotted against the ratio $\bar{a}/\bar{d}_S$. The maximum of a standard distribution, representing the experiments (Bilicki 1987), differed from the calculation based on the cubic model by 10, whereas the standard deviation of the measurements was 25%. In the face of this result, we adopted the following correlation:

$$\frac{\bar{a}}{\bar{d}_S} = \frac{1.6}{\alpha^{1/3}} - 1. \qquad [7]$$

Since transition is postulated to occur when

$$\frac{\bar{l}}{\bar{d}} = \frac{\bar{a}}{\bar{d}_S}, \qquad [8]$$

and when the limiting value α_* corresponds to the correlation in [7], we can write the implicit equation

$$\frac{1.6}{\alpha_*^{1/3}} - 1 = A_1 \frac{C_D^{1/2} U_\infty^{3/2}}{v_*^{3/2}} \qquad [9a]$$

or

$$\frac{1.6}{\alpha_*^{1/3}} - 1 = A_1 \frac{C_D^{1/2}}{v_*^{3/2}} \left(\frac{U_{GS}}{\alpha_*} - \frac{U_{LS}}{1-\alpha_*} \right)^{3/2}. \qquad [9b]$$

The boundary between bubble and slug flow is governed by [9b] together with [5] in which α is replaced by its limiting value α_*. These two equations contain the unknowns v_*, U_{LS}, U_{GS} and α_*, and in order to arrive at the required locus in U_{LS}, U_{GS} coordinates, we supplement the system of equations with the momentum balance equation proposed by Ishii & Zuber (1979). Adapted to our case, we write

$$\frac{U_{GS}}{\alpha_*} - \frac{U_{LS}}{1-\alpha_*} = \left[\frac{4}{3} \bar{d}_S \frac{g}{C_D} \frac{\rho_L - \rho_G}{\rho_L} (1-\alpha_*) \right]^{1/2}. \qquad [10]$$

The value of the product $A_1 C_D^{1/2}$ which appears in [9b] has been so adjusted as to cause the locus U_{GS}, U_{LS} to pass through a single experimental point measured by Bilicki (1987). With

$$\alpha = 0.34,\ U_{LS} = 0.35\ \text{m/s and}\ U_{GS} = 0.23\ \text{m/s}$$

we obtain

$$A_1 C_D^{1/2} = 0.527. \qquad [11]$$

The flow-pattern boundary under discussion has been calculated numerically with the aid of [5], [9b] and [10] with the constant value [11], and is shown in figures 5–8. Figure 5 corresponds to $D = 20$ mm, with $d_S = 2$ mm, and a flow of air in water, so that $\rho_L = 1000\ \text{kg/m}^3$ and

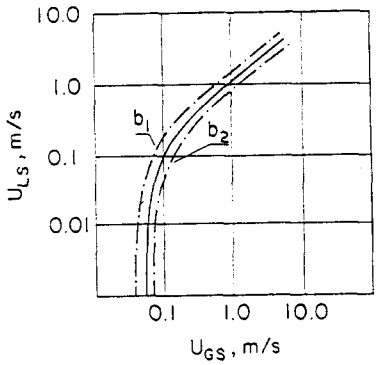

Figure 5. Calculated boundary between bubble and slug flow. The —·— lines b_1, b_2 correspond to a deviation of ±15%.

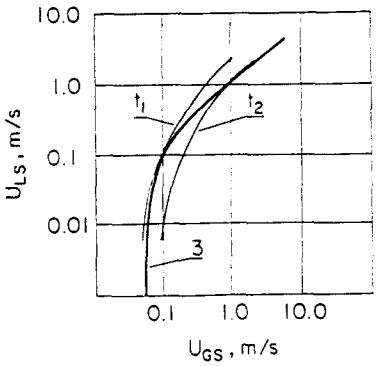

Figure 6. Comparison between the present result, curve 3, and the experimental range t_1, t_2 reported by Bilicki (1987).

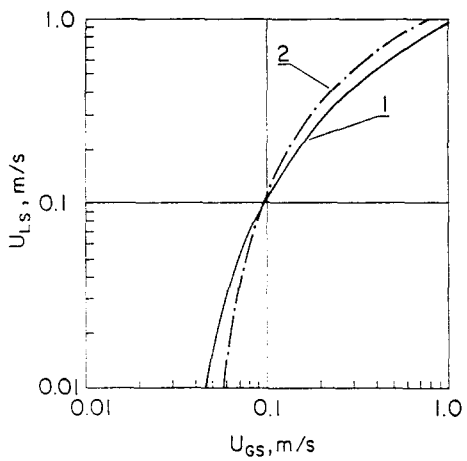

Figure 7. Effect of bubble diameter on the boundary: 1, $d_S = 3$ mm; 2, $d_S = 1$ mm.

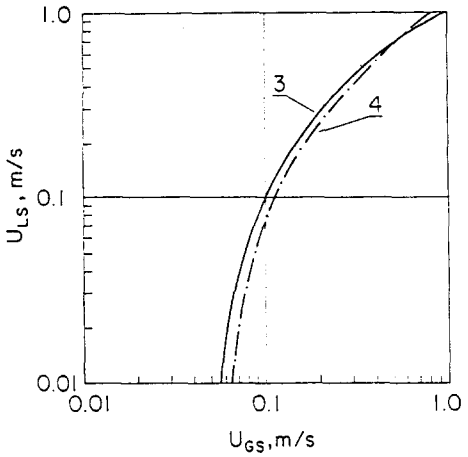

Figure 8. Effect of pipe diameter: 3, $D = 20$ mm; 4, $D = 50$ mm.

$\rho_G = 1.25$ kg/m^3. The baseline corresponds to $\bar{a}/\bar{d}_S = (\bar{a}/\bar{d}_S)_*$ satisfying [7]; lines b_1 and b_2 correspond to

$$\frac{\bar{a}}{\bar{d}_S} = (1 \pm 0.15)\left(\frac{\bar{a}}{\bar{d}_S}\right)_*; \qquad [12]$$

that is, to the limits dictated by experiment for a standard deviation of 25% and a confidence level of 0.9.

Figure 6 compares the calculated result, curve 3, with the experimental range t_1, t_2 reported by Bilicki (1987). It appears that the proposed correlation constitutes a reasonable representation of the experimental results.

The analytically derived correlation enables us now to assess the sensitivity of the predicted boundary to changes in some of the parameters. Figure 7 shows the influence of bubble diameter with $d_S = 3$ mm (curve 1) and 1 mm (curve 2), respectively. The effect of pipe diameter results in the change from curve 3 ($D = 20$ mm) to curve 4 (50 mm); depicted in figure 8. Finally, figure 9 illustrates the effect of a density ratio change from $\rho_L/\rho_G = 800$ (air—curve 3) to $\rho_L\rho_G = 5$ (steam—curve 4). Curve 3 here is the same as curve 3 in figure 6 and the base curve in figure 5. Figure 10 shows a comparison of the present analytic correlation—curve 3—with that of Taitel *et al.* (1980)—curve 6. In spite of the large differences in the approach to the problem, the two results are indistinguishable to all intents and purposes.

The last diagram in this set, figure 11, compares our analytic results with those of the same experimenters as exhibited by Bilicki (1987). Since the other authors did not supply sufficient details of the conditions encountered in their experiments, we plot them against those curves from our

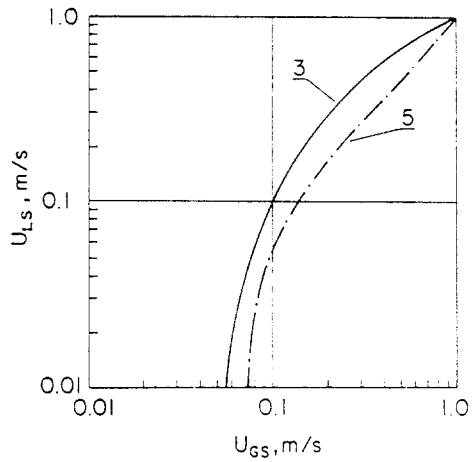

Figure 9. Effect of fluid densities: 3, $\rho_L = 1000\ kg/m^3$, $\rho_G = 1.25\ kg/m^3$; 5, $\rho_L = 500\ kg/m^3$, $\rho_G = 100\ kg/m^3$.

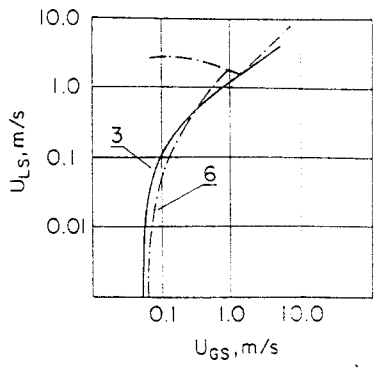

Figure 10. Comparison between the present result (curve 3, from figures 5, 6, 8, and 9) and that due to Taitel *et al.* (1980) (curve 6).

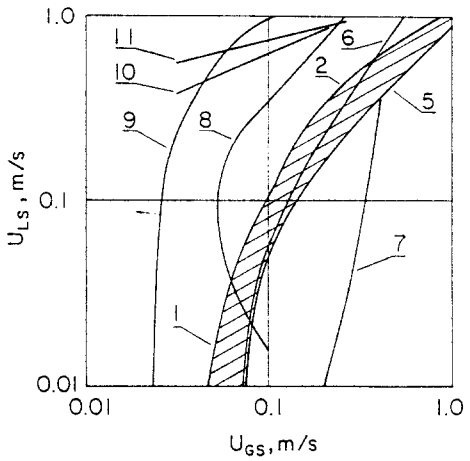

Figure 11. Comparison of the present analytic results with the boundaries recommended by other investigators. 1, Present result, $D = 20$ mm, $d_S = 3$ mm; air–water ($\rho_L/\rho_G = 800$). 2, Present result, $D = 20$ mm, $d_S = 1$ mm; air–water ($\rho_L/\rho_G = 800$). 5, Present result, $D = 20$ mm, $d_S = 2$ mm; steam–water ($\rho_L/\rho_G = 5$). 6, Taitel *et al.* (1980). 7, Govier & Aziz (1972). 8, Griffith & Wallis (1961). 9, Sternling (1965). 10, Gould (1974). 11, Oshinowo & Charles (1974).

figures 5–10 which encompass the widest field of the diagram covered by the range of parameters discussed in this paper. This comparison merely confirms the remarks made in the introduction to the effect that most probably several influences still remain to be discovered. Nevertheless, the coincidence between our analysis, that of Taitel *et al.* and the experimental results of Bilicki and Taitel *et al.* lends an aura of plausibility to the present (and Taitel's!) analytic formulation.

3. TRANSITION FROM SLUG TO FROTH FLOW

3.1. General Remarks

The diagram in figure 12 shows a schematic of slug flow, i.e. of the configuration in which gas- or vapor-filled Taylor bubbles move axially in a statistically distributed linear array. Two consecutive bubbles are separated by a liquid plug. On the basis of observation, we postulate that transition to froth flow may occur by one of two mechanisms. For the first, we postulate a mechanism of coalescence of Taylor bubbles similar to the one discussed for spherical-bubble flow. This is a statement that a Taylor bubble which approaches the one ahead of it by a distance l lower than a characteristic length l_*, figure 12, will be forced by the flow field to catch up and coalesce

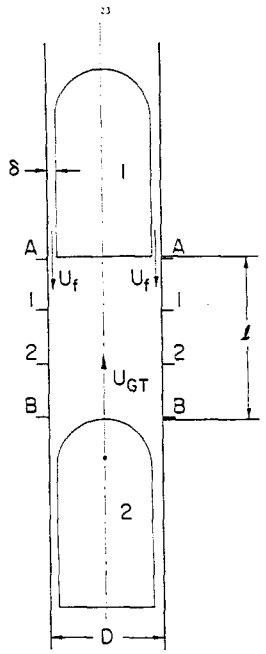

Figure 12. Slug-flow configuration.

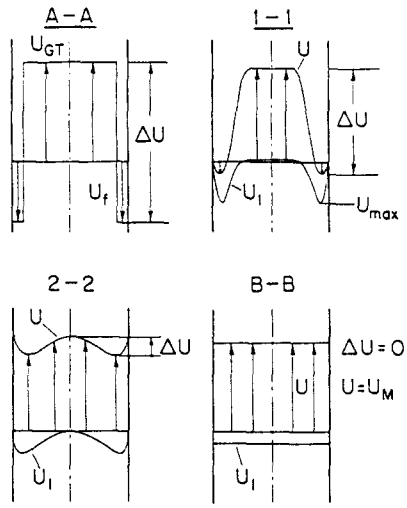

Figure 13. Evolution of velocity profiles in a plug.

with its predecessor. When this occurs, the slug-flow pattern gives way to froth flow. The critical length l_* of l is characterized by the fact that the maximum velocity difference ΔU in the velocity distribution at level B-B induced in the liquid by the presence of bubble No. 1 has become equal to the friction velocity v_* because the latter is a measure of local turbulent fluctuations.

The second possible mechanism of flow-regime change is that of onset of instability in the thin cylindrical layer of thickness δ which is formed between the Taylor bubble and the tube wall. This we base on the theory of thin liquid films (Moissis 1963; Milne-Thomson 1950). Of the two mechanisms, the second causes transition if film instability sets in when the distance between two Taylor bubbles exceeds the critical value l_*.

3.2. The Mechanism of Coalescence

The velocity distributions in the plug between sections A-A and B-B of figure 12, are modifications of the basic volumetric velocity whose mean value is

$$U_M = U_{LS} + U_{GS}. \qquad [13]$$

The evolution of the velocity distributions in the plug is shown sketched in figure 13; the consecutive velocity profiles can all be regarded as evolving from the flow field in cross section A-A.

We assume for a moment that the plug is stationary and consider the fluid issuing from the annulus of gap δ whose mean velocity with respect to the tube we denote by U_f. This flow constitutes a wall jet of small width δ wetting the tube of comparatively large diameter D. Thus, we can neglect the curvature and employ the theory of 2-D jets (Schlichting 1979, pp. 732–733) to determine the dimensional structure of the equation governing the evolution of velocity. The wall jet produces a very thin boundary layer near the wall and away from it projects a stream which has the character of a 2-D jet. Denoting this velocity by U_1, we find that its maximum can be written (Schlichting 1979, pp. 732–733) as

$$U_{max}(z) = \text{const} \times \left(\frac{J}{z\rho}\right)^{1/2}. \qquad [14]$$

Neglecting the boundary layer, we estimate the momentum of the flow J, as

$$J = \rho \int_{A_f} U_f^2 \, dA \sim \rho U_f^2 \delta, \qquad [15]$$

where A_f is the area of the annulus with respect to a unit diameter. Hence,

$$U_{max}^2(z) \sim \delta \frac{U_f^2}{z}. \qquad [16]$$

In actual fact the Taylor bubble is not stationary and the velocity profile in cross section A-A is augmented by the air or vapor velocity, U_{GT}, of the bubble, giving a velocity difference ΔU.

The velocity U_{GT} has been investigated by Davies & Taylor (1950), Moissis & Griffith (1962) and, more recently, by Bendiksen (1985). We can assume here the relation

$$U_{GT} = 1.2\,(U_{LS} + U_{GS}) + C[gD(\rho_L - \rho_G)\rho_L]^{1/2}, \qquad [17a]$$

with

$$C = 0.35 + 2.8 \exp\left(-1.06 \frac{l}{D}\right). \qquad [17b]$$

The modulation of the velocity profile postulated for cross section A-A is sketched in figure 13 for sections 1-1, 2-2 and B-B of figure 12. In each profile we discern the existence of a velocity maximum in the center and a velocity minimum in the annulus, the difference ΔU decreasing with ζ measured away ($d\zeta = -dz$) from A-A in accordance with the same relation as that postulated for a Taylor bubble at rest. Hence,

$$\Delta U = (U_{GT} + U_f)\left(\frac{\delta}{z}\right)^{1/2}. \qquad [18]$$

In order to relate the velocity profile implied by [16]–[17] to the basic flow in the channel, [13], we apply the continuity equation for the plug, ignoring the gas bubbles that are observed in it. Thus at level A-A, we write

$$\rho_L(U_{LS} + U_{GS})\,A = \rho_L[U_f A_f + U_{GT}(A - A_f)]. \qquad [19]$$

In any other cross section, we have

$$\rho_L A(U_{LS} + U_{GS}) = \rho_L \int_A U \, dA. \qquad [20]$$

Here $A = \pi D^2/4$ is the total area, and A_f is the area of the annulus of width δ. By an obvious transformation, we calculate from [19] that

$$U_f = \frac{U_{GT}(D\text{-}2\delta)^2 - D^2(U_{LS} + U_{GS})}{4\delta(D\text{-}\delta)},$$

or, for $\delta \ll D$, we simplify this to

$$U_f = \frac{U_{GT} - (U_{LS} + U_{GS})}{\left(\frac{4\delta}{D}\right)}. \qquad [21]$$

To derive the criterion based on the comparison

$$\Delta U = v_* \qquad [22]$$

mentioned earlier, we fall back on [5] in which U_{LS} is replaced by $U_{LS} + U_{GS}$ and in which the void fraction is retained, realizing that its value in the plug is small, but that the presence of bubbles is essential for the creation of the level of turbulence which corresponds to v_*.† Hence,

$$v_* = U_M \left\{ \frac{\left[\frac{1}{2} f(1-\alpha^2) + \alpha(1-\alpha)\left(1 - \frac{\rho_G}{\rho_L}\right)\frac{Dg}{U_M^2}\right]}{\left(1 + 1.5\alpha \frac{D}{d_b}\right)} \right\}^{1/2}. \qquad [23]$$

†In subsequent calculations we put $\alpha = 0.04$ and $d_b = 2$ mm.

From [22] and [18], we deduce the following formula for the critical length:

$$l_* = \frac{A_2(U_f + U_{GT})^2\,\delta}{v_*^2}. \qquad [24]$$

Here A_2 is an adjustable constant to be determined later. It follows that transition occurs when the dimensionless distance l (referred to D) between bubbles becomes

$$\frac{l}{D} \leqslant \left[\frac{A_2(U_f + U_{GT})^2}{v_*^2}\right]\left(\frac{\delta}{D}\right). \qquad [25]$$

In order to complete the calculation, it is necessary to adopt a hypothesis concerning the film thickness δ. We base it on the work of Özgü *et al.* (1973), and assume

$$\delta = 1.5\left(\frac{3\nu_L U_f}{g}\right)^{1/2}. \qquad [26]$$

The boundary between plug and froth flow can now be calculated numerically in the coordinates U_{LS} vs U_{GS} with l_*/D as a parameter. To this end, we utilize the five equations [17a], [21], [23], [25] and [26] which contain the five unknowns U_f, U_{GT}, v_*, δ, $(U_{LS} + U_{GS})$ and the parameter l_*/D. Figure 14 contains several boundaries of this kind. The constant A_2 is adjusted for the boundary to pass through one experimental point measured by Bilicki (1987). This was given by $U_{LS} = 0.01$ m/s, $U_{GS} = 0.9$ m/s, $l_*/D = 7$; and resulted in

$$A_2 = 0.35. \qquad [27]$$

A similar criterion for the transition under discussion was utilized by Taitel *et al.* (1980) with the pipe entry length as a parameter. We suggest that our parameter l_*/D plays the same role as an entry length. This conviction is based on the observation that points on a given l_E/D curve (l_E = entry length) in Taitel *et al.* determine the flow conditions for which slug flow is about to change to froth flow.

3.3. The Instability Mechanism

The detailed theory of the second mechanism is based on the assumptions that:

(a) the flow in the film is potential;

(b) the perturbation amplitude is small;

and

(c) the inertial forces in the film may be neglected.

The equation of motion in the film is

$$\frac{\partial \Psi}{\partial x} = \frac{\partial \eta}{\partial t} - \frac{\partial \Phi}{\partial x}\frac{\partial \eta}{\partial x}, \qquad [28a]$$

in which Ψ and Φ are the stream and potential functions, respectively, and η denotes the perturbation amplitude.

Instabilities are due to the fact that the liquid film is excited externally by a flow of vapor or gas of velocity U_{GT} and causes it to assume a wavy form. The potential equation [28] possesses a real solution for η, provided that

$$U_{GT} + U_f \leqslant U_{lim} \text{ (algebraic sum)}, \qquad [28b]$$

where

$$U_{lim} \sim \left(\frac{\sigma}{\rho_G \delta}\right)^{1/2}. \qquad [29]$$

Here σ denotes the surface tension of water in the presence of air or steam, as the case may be. This relation is based on the same assumptions as those postulated by Feldman (1957); it was successfully employed by Mossis (1963), who claimed that the most unstable film occurs when its length $\lambda = 10\delta$. The experimental investigation carried out by Bilicki (1987) confirms the fact of transition from plug to froth flow and demonstrates that the limiting velocity U_{lim} additionally

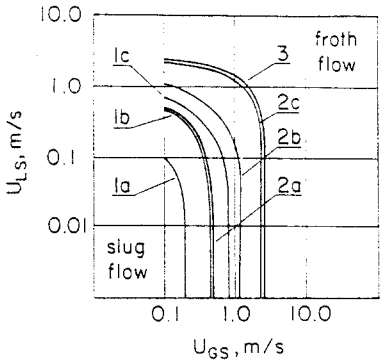

Figure 14. Boundary between slug flow and froth flow. 1a, $l_*/D = 3$; $D = 20$ mm. 1b, $l_*/D = 5$; $D = 20$ mm. 1c, $l_*/D = 7$; $D = 20$ mm. 2a, $l_*/D = 3$; $D = 50$ mm. 2b, $l_*/D = 5$; $D = 50$ mm. 2c, $l_*/D = 7$; $D = 50$ mm. 3, $l_*/D > 7$, based on film stability.

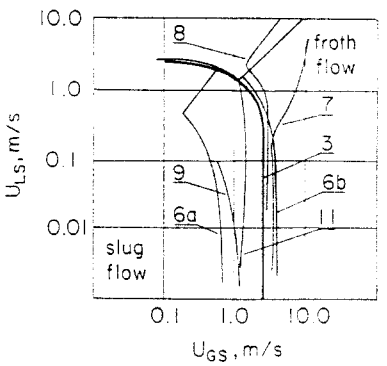

Figure 15. Slug–froth transition. Comparison between the present result and those of other investigators. 3, Present result, $l_*/D > 7$ (stability theory) 6a, Taitel *et al.* (1980), $L_E/D = 50$; $D = 25$ mm. 6b, Taitel *et al.* (1980), $L_E/D = 200$; $D = 50$ mm. 7, Govier & Aziz (1972). 8, Griffith & Wallis (1980). 9, Sternling (1965). 11, Oshinowo & Charles (1974).

depends on the pipe diameter D. This means that the constant for [29] must display it. To retain dimensional homogeneity we put

$$U_{\text{lim}} = A_3\left(\frac{D}{2\delta}\right)\left(\frac{\sigma}{\rho_G \delta}\right)^{1/2}. \qquad [30a]$$

Once again, Bilicki's work leads to the value

$$A_3 = 0.1. \qquad [30b]$$

The locus defined by [30a] with $U_{GT} + U_f$ from [28b] expressed with the aid of [29] is shown plotted in figure 14, curve 3. This locus is congruent to the curves $l/l_* = \text{const}$ and corresponds to $(l_*/D) \gtrsim 7$.

The comparison between our results and those of other investigators, figure 15, shows good agreement as far as the general geometric shape of the locus is concerned. Beyond that we can only reiterate the remarks made at the end of section 2, and to conclude that all results taken together do not yet amount to a scientific solution of the problem.

4. TRANSITION FROM FROTH TO ANNULAR MIST FLOW

For the sake of completeness, we recall that in order to determine the criterion for the transition from froth to annular mist flow, it is usual to consider fully-developed annular flow and to determine the dynamic conditions under which the thin film of thickness δ can be sustained in its upward flow by the shearing stress τ_s produced by the faster-moving vapor stream. The condition for annular flow to persist has been studied by Wallis & Makkenokery (1974) and Pushkina

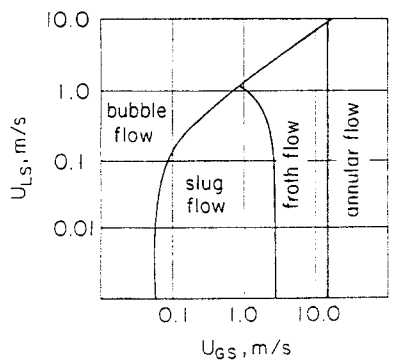

Figure 16. Transition "map" for the upward flow of air in water with $D = 20$ mm, $d_S = 2$ mm, $l_*/D > 7$.

& Sorokin (1969). Dimensional analysis shows that the phenomenon is governed by the Kutateladze number,

$$\mathrm{Ku} = U_{GS}\,\rho_G^{1/2}\,[g\sigma(\rho_L - \rho_G)]^{-1/4}. \quad [31]$$

Annular mist flow is possible when

$$\mathrm{Ku} > 3.2, \quad [32]$$

and below that value flooding occurs and froth flow persists.

5. SUMMARY

Figure 16 gives an idea of the type of "map" implied in the preceding equations; it was drawn for an upward flow of air in water with $D = 20\,\mathrm{mm}$, $d_S = 2\,\mathrm{mm}$ and $l_*/D > 7$.

Acknowledgements—The work described in this paper was performed under Grant DE-AC02-84ER-13167 awarded to Brown University of the Office of Basic Energy Sciences of the U.S. Department of Energy. Z. Bilicki expresses his appreciation for the invitation to spend his study leave in the U.S.A. Special thanks for his encouraging attitude are due to the project Manager, Dr O. P. Manley.

REFERENCES

BENDIKSEN, K. H. 1985 On the motion of long bubbles in vertical tubes. *Int. J. Multiphase Flow* **11,** 797–812.

BILICKI, Z. 1987 Experimental investigation of certain aspects of upward vertical bubble and slip flows. To be published.

DAVIES, R. M. & TAYLOR, G. I. 1950 The mechanics of large bubbles rising through extended liquids and through liquids in tubes. *Proc. R. Soc. Lond.* **200A,** 375–390.

FELDMAN, S. 1957 On the hydrodynamic stability of two viscous incompressible fluids in parallel uniform shearing motion. *J. Fluid Mech.* **2,** 343–370.

GOULD, T. L. 1974 Vertical two-phase steam–water flow in geothermal wells. *J. Petrol. Technol.* **26,** 833–842.

GOVIER, G. W. & AZIZ, K. 1972 *The Flow of Complex Mixtures in Pipes.* Van Nostrand-Reinhold, New York.

GRIFFITH, P. & WALLIS, G. B. 1961 Two-phase slug flow. *J. Heat Transfer* **83,** 307–320.

ISHII, M. & ZUBER, N. 1979 Drag coefficient and relative velocity in bubbly, droplet or particulate flows. *AIChE Jl* **25,** 843–855.

MILNE-THOMSON, L. M. 1950 *Theoretical Hydrodynamics*, 2nd edn. Macmillan, New York.

MOISSIS, R. 1963 The transition from slug to homogeneous two-phase slug flow. *J. Heat Transfer* **85,** 366–370.

MOISSIS, R. & GRIFFITH, P. 1962 Entrance effects in two-phase slug flow. *J. Heat Transfer* **84,** 29–39.

OSHINOWO, T. & CHARLES, M. T. 1974 Vertical two-phase flow: Part I. Flow pattern correlations. *Can. J. chem. Engng* **52,** 25–35.

ÖZGÜ, M. R., CHEN, J. C. & STENNING, A. H. 1973 Local liquid film thickness around Taylor bubbles. *J. Heat Transfer* **95,** 425–427.

PUSHKINA, O. L. & SOROKIN, YU. L. 1969 Breakdown of liquid film motion in vertical tubes. *Heat Transfer Sov. Res.* **1**(5), 56–64.

SCHLICHTING, H. 1979 *Boundary-layer Theory*, 7th edn. McGraw-Hill, New York.

SEKOGUCHI, K., FUKUI, H. & SATO, Y. 1981 Flow characteristics and heat transfer in vertical bubble flow. In *Two-phase Flow Dynamics* (Edited by BERGLES, A. E. & ISHIGAI, S.), pp. 59–74. Hemisphere, Washington, D.C.

STERNLING, V. C. 1965 Two-phase flow theory and engineering decision. Award lecture presented at *AIChE A. Mtg.*

TAITEL, Y., BORNEA, D. & DUKLER, A. E. 1980 Modelling flow pattern transitions for steady upward gas–liquid flow in vertical tubes *AIChE Jl* **26,** 345–354.

THEOFANOUS, T. G. & SULLIVAN, J. 1982 Turbulence in two-phase dispersed flow. *J. Fluid Mech.* **116,** 343–362.

WALLIS, G. B. & MAKKENOKERY, S. 1974 The hanging film phenomena in vertical annular two-phase flow. *J. Fluids Engng* **96,** 297–298.